CHAPTER 5

Approaching Control Based on a Distributed Tether Model

Before performing the on-orbit service mission, the TSR should arrive at the desired position in the neighborhood area of the target and keep a stable relative attitude. Therefore how to control the TSR to approach the target and maintain the attitude is one of the key techniques of this system. Given the limited fuel carried on the terminal operation robot, the cost of fuel is regarded as one of the most important factors during the controller design of position and attitude. To reduce the fuel consumption in the approaching phase, various coordinated controllers are investigated in the literature.

Masahiro considered the attitude control of the terminal operation robot using moving links connected with the tether and verified the designed controller by experiments [1]. However, to simplify problems, he assumed the tether to be a massless rod and very short in his studies. Yuya discussed the collaborative control of the position of the operational robot in the approaching phase using the tension along the tether and the thrust acting on the robot, whereas the attitude of the robot was not considered [2]. Mori designed a coordinated scheme which used tether tension and thrust for control of the tethered satellite cluster systems. He proved that the proposed controller could reduce the fuel consumption and improved control precision [3]. Godard also used the same assumption as Masahiro and established a coordinated fault-tolerant nonlinear control frame to control the attitude of a satellite by moving the tether attachment point [4]. Even though the tether was involved in these studies, they all assumed it to be a massless rod and neglected the distributed mass of the tether and the force acting on the tether. Besides, they only considered one aspect of orbit and attitude control. However, the distributed mass of the tether and the distributed force acting on the tether will remarkably degrade the precision of the coordinate controller, especially when the tether mass is close to or heavier than the mass of the operational robot. Meanwhile, because of the coupling between the attitude and the position, a great disturbing force is likely to occur, which will lead to more fuel consumption and even the instability of the whole system.

Tethered Space Robot
https://doi.org/10.1016/B978-0-12-812309-6.00005-1

To overcome the problems of the controllers designed in the literature, the massless rod model should be improved at first with the consideration of the attitude, the position of the operation robot, the distributed mass of the tether, and the distributed force acting on the tether simultaneously. This requires reference to the classical methods used in the dynamics modeling of tethered satellites. Presently, there are mainly three kinds of dynamical models for tethered satellites: (1) the rod model, (2) the lumped mass model, (3) the continuum model. The rod model converts the stretched tether into an equivalent rod. Since the space tether usually needs to keep certain tension, this simplification is reasonable in most cases and is widely used in the control of tethered satellites. Besides, according to the different application conditions, the model also has different forms. The flexibility and mass of the tether are ignored in the study of the drift control of geostationary tethered satellites in Anderson and Hagedorn [5]. Misra considered the effects of varying the tether mass by introducing the equivalent system mass [6]. Williams further investigated the flexibility of the tether when using the long tether to capture an in-plane payload [7]. However, these models all regard the terminal mechanism as a mass point. This is not suitable for the tethered space robot system because the operation robot usually needs to adjust its attitude which may be affected by the tether tension during the phase of approaching targets. The lumped mass model discretizes the continuous tether into a series of mass points that are connected by massless flexible rods [8,9]. This model can be used to simulate the dynamical behavior of tethered systems, but it is too complex for the controller design of the deploying tethered space robot. The continuous model usually employs the Hamilton principle to build the complete system dynamic model at first, and then uses the Ritz method, the Galerkin method, or the finite element method to discretize the continuous tether [10–12]. By using these methods, the motion of tethered systems can be calculated precisely, but the models obtained by discretizing the tether with high order functions or dividing it into many segments will also be too complex for the controller design.

In this chapter, the pose coupling dynamics modeling and the minimum-fuel coordinated controller for the tethered space robot system in the approaching phase are considered. Firstly, the Hamilton principle is employed to obtained the complete dynamics model of the tethered space robot system. Then, assuming the passive deployment mechanism will keep a certain level of tension in the tether, the first order linear function is used to approximate the shape of the tether. Meanwhile, the flexibility of the tether is neglected. The coupling dynamics model can be derived by using the

selected approximation function to discretize the complete dynamics model. Then a new optimal coordinated controller is designed based on the model. The hp-adaptive pseudospectral method is used to calculate the open-loop ideal inputs and states corresponding to the minimum fuel trajectory, and the PD controller to adjust the system inputs to ensure the actual states to track the ideal states. Finally, the proposed method is validated by comparison between the proposed method and the traditional method based on the massless rod model.

5.1 DYNAMICS MODELING OF TSR

This section focuses the coupling dynamics modeling and coordinated control problems of the TSR system during the approaching phase. Assume thrusters are used to control the orbit and attitude of the operation robot. Because the fuel for thrusters is limited, it is of great importance to consider the tether in the design of the pose controller to reduce the fuel consumption.

Regarding the tethered space robot system in the approaching phase, assume the platform is far heavier than the flexible tether and the operation robot, the influence on the platform caused by the movements of the tether and the operation robot can be neglected. Therefore the platform is simplified to be a mass point. Also, the mass center of the whole system is assumed to coincide with the mass center of the space platform and moves along a nearly circular Keplerian orbit. As for the space tether, since the length is far bigger than the cross-sectional diameter, its torsion and bending stiffness are neglected, and it is simplified to be an arc with a variable length. Furthermore, it is assumed that the target and the platform are in the same orbit plane. Therefore in the approaching phase, the operation robot only is assumed to move in the orbit plane, while the out-plane motion can be neglected. Besides, since the rolling motion is decoupled with other forms of motion and is separately controlled by the stabilization loop, it is also neglected in this research. Therefore this investigation is to study the in-plane motion control problem of the flexible tether and the operation robot. Under these assumptions introduced above, a simplified system is acquired and shown in Fig. 5.1 [13].

To describe the in-plane motion of the tethered space robot system, three reference frames are introduced:

(1) The inertial frame $Ox_e y_e z_e$: the origin O is located in the center of the earth; the x_e axis is towards the ascending point of the orbit; the

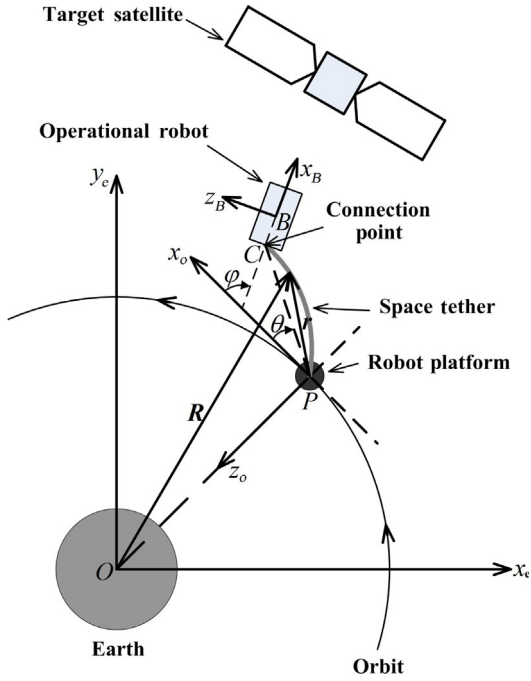

Fig. 5.1 Simplified sketch map of TSR.

z_e axis has the same direction as the normal vector of the orbit plane; the y_e axis completes the frame following the right-hand principle.

(2) The orbital frame $Px_oy_oz_o$: the origin P is located in the mass center of the space platform; the x_o axis has the same direction as the tangent vector of the orbit; the z_o axis is directed from the origin P to the earth center O; the y_o axis has the same direction as the negative normal vector of the orbit plane.

(3) The body frame $Bx_By_Bz_B$: the origin B is located in the mass center of the terminal operation mechanism; the x_B axis is directed from the tether attachment point C to the mass center B; the y_B axis has the same direction as the negative normal vector of the orbit plane; the y_e axis completes the frame following the right-hand principle.

To describe the motion of the space tether, the unstrained arc-length coordinate s, which represents the length of the unstrained tether between a point on the tether and one end of the tether, is introduced. To facilitate the computation, we set the end to be stored in the space platform as the

zero point. Also, $\xi(t)$ and L are used to represent the coordinates of the tether deploying point on the platform and another end of the tether, respectively. Then, according to the classical string theory, the stain $\varepsilon(s,t)$ and tangent vector $\boldsymbol{\tau}(s,t)$ in the tether must satisfy formulas (5.1) and (5.2), respectively:

$$\varepsilon(s,t)=\left\|\frac{\partial \boldsymbol{R}}{\partial s}\right\|-1=\left\|\frac{\partial \boldsymbol{r}}{\partial s}\right\|-1 \quad (\xi\le s\le L) \tag{5.1}$$

$$\boldsymbol{\tau}(s,t)=\frac{\partial \boldsymbol{R}}{\partial s}\Big/\left\|\frac{\partial \boldsymbol{R}}{\partial s}\right\|=\frac{\partial \boldsymbol{r}}{\partial s}\Big/\left\|\frac{\partial \boldsymbol{r}}{\partial s}\right\| \quad (\xi\le s\le L) \tag{5.2}$$

where $\boldsymbol{R}$ and $\boldsymbol{r}$ are the position vectors of a point on the inertial frame and the orbital frame, respectively.

5.1.1 Dynamics Modeling Based on the Hamiltonian Theory

The tethered space robot system can be structurally divided into four parts, that is, the deployed tether, the space platform, the stored tether and the operation robot. Therefore its kinetic energy T can be given as:

$$\begin{aligned}T=&\int_{\xi}^{L}\frac{1}{2}\mu\dot{\boldsymbol{R}}^{\mathrm{T}}\dot{\boldsymbol{R}}\,\mathrm{d}s+\frac{1}{2}m_P\dot{\boldsymbol{R}}_P^{\mathrm{T}}\dot{\boldsymbol{R}}_P+\frac{1}{2}\mu\xi\dot{\boldsymbol{R}}_P^{\mathrm{T}}\dot{\boldsymbol{R}}_P\\&+\frac{1}{2}m_B\dot{\boldsymbol{R}}_B^{\mathrm{T}}\dot{\boldsymbol{R}}_B+\frac{1}{2}I_B(\dot{\varphi}-\omega)^2\end{aligned} \tag{5.3}$$

where μ denotes the mass density of the tether per unit arc-length, m_P and m_B are the mass of the space platform and the operation robot, I_B is the moment of inertia about the γ_B axis, ω is the orbit angular velocity, $\boldsymbol{R}_P$ and $\boldsymbol{R}_B$ are the position vectors in the inertial frame at points P and B, respectively. Its potential energy V can be computed as:

$$V=\int_{\xi}^{L}\left(V_\varepsilon-\mu\frac{GM}{\|\boldsymbol{R}\|}\right)\mathrm{d}s-m_P\frac{GM}{\|\boldsymbol{R}_P\|}-\mu\xi\frac{GM}{\|\boldsymbol{R}_P\|}-m_B\frac{GM}{\|\boldsymbol{R}_B\|} \tag{5.4}$$

where G is the universal gravitational constant, M is the mass of the earth, V_ε is the elastic potential energy of the tether. According to the theory of elastic, V_ε can be obtained as:

$$V_\varepsilon(s,t)=\frac{1}{2}EA\varepsilon(s,t)^2$$

where E is the Young's module of the tether, A is the cross-sectional area. The nonconservative forces in the TSR include the damping force in the

tether, the control forces and torques acting on the platform and the operation robot. Therefore the virtual work δW of nonconservative forces can be computed as:

$$\delta W = \int_{\xi}^{L} (-N_{\mathrm{D}}\delta\varepsilon)\mathrm{d}s + \delta \boldsymbol{R}_P^{\mathrm{T}}\boldsymbol{F}_P + \delta \boldsymbol{R}_B^{\mathrm{T}}\boldsymbol{F}_B + M_B\delta\varphi \tag{5.5}$$

where δ is the variational operator, $\boldsymbol{F}_P$ and $\boldsymbol{F}_B$ are the control forces acting on the space platform and the operation robot, respectively, M_B is the attitude control torque acting on the operation robot, N_{D} is the damping force existing in the tether. According to the linear Kelvin-Voigt law of viscoelasticity, N_{D} can be expressed as:

$$N_{\mathrm{D}} = \alpha EA\dot{\varepsilon} \tag{5.6}$$

where α is the damping coefficient of the tether.

The equations of motion for the TSR system may be derived by a straightforward application of the Hamilton principle:

$$\int_0^t (\delta T - \delta V + \delta W)\mathrm{d}t = 0 \tag{5.7}$$

By inserting Eqs. (5.3)–(5.5) into Eq. (5.7) and then performing partial integral with respect to time t, the weak form equations representing the dynamics of the TSR system can be written as:

$$\int_0^t \left\{ \int_{\xi}^{L} \left(-\mu \boldsymbol{A}^{\mathrm{T}}\delta\boldsymbol{R} - \boldsymbol{n}^{\mathrm{T}}\delta\boldsymbol{R}'\right)\mathrm{d}s + \delta\boldsymbol{R}_P^{\mathrm{T}}\left[-(m_P + \mu\xi)\boldsymbol{A}_P - \mu\dot{\xi}^2\frac{\partial \boldsymbol{R}(\xi)}{\partial s} + \boldsymbol{F}_P\right] \right.$$
$$\left. + \delta\boldsymbol{R}_C^{\mathrm{T}}[-m_B\boldsymbol{A}_B + \boldsymbol{F}_B] + \delta\varphi[-I_B\ddot{\varphi} + M_B] \right\}\mathrm{d}t = 0 \tag{5.8}$$

where $\boldsymbol{n}$ is the tension vector in the tether which can be expressed as:

$$\boldsymbol{n}(s,t) = EA[\varepsilon(s,t) + \alpha\dot{\varepsilon}(s,t)]\boldsymbol{\tau}(s,t) \tag{5.9}$$

$\boldsymbol{A}$ is the maneuvering acceleration caused by forces except for the gravitation which can be calculated as:

$$\boldsymbol{A} = \ddot{\boldsymbol{R}} + \frac{GM}{\|\boldsymbol{R}\|^3}\boldsymbol{R} \tag{5.10}$$

$\boldsymbol{A}_P$ and $\boldsymbol{A}_B$ are maneuvering accelerations at point P and point B, respectively. Considering the property of the variational operation, Eq. (5.9) can be further simplified as the following form:

$$\int_{\xi}^{L}\left(-\mu\boldsymbol{A}^{\mathrm{T}}\delta\boldsymbol{R}-\boldsymbol{n}^{\mathrm{T}}\delta\boldsymbol{R}'\right)\mathrm{d}s+\delta\boldsymbol{R}_{P}^{\mathrm{T}}\left[-(m_{P}+\mu\xi)\boldsymbol{A}_{P}-\mu\dot{\xi}^{2}\boldsymbol{R}'(\xi)+\boldsymbol{F}_{P}\right]$$
$$+\delta\boldsymbol{R}_{C}^{\mathrm{T}}[-m_{B}\boldsymbol{A}_{B}+\boldsymbol{F}_{B}]+\delta\varphi[-I_{B}\ddot{\varphi}+M_{B}]\equiv 0 \tag{5.11}$$

Since vector $\boldsymbol{R}$ involves the orbital motion of the TSR system, Eq. (5.11) cannot be directly used to describe the motion during the approaching phase. Therefore Eq. (5.11), which is in the inertial frame, needs to be transformed into the orbital frame $Px_{o}y_{o}z_{o}$. From Fig. 5.3, we have

$$\boldsymbol{R}=\boldsymbol{r}+\vec{OP} \tag{5.12}$$

Also, according to the Clohessy-Wiltshire equation, the maneuvering acceleration $\boldsymbol{A}$ can be calculated as:

$$\boldsymbol{A}=\begin{bmatrix}\ddot{x}-2\omega\dot{z}\\ \ddot{z}+2\omega\dot{x}-3\omega^{2}z\end{bmatrix} \tag{5.13}$$

where x and z are the coordinates of a point the orbital frame, which means the position vector can be written as $\boldsymbol{r}=[x\ \ z]^{\mathrm{T}}$. Inserting Eq. (5.13) into Eq. (5.11) yields:

$$\int_{\xi}^{L}\left(-\mu\boldsymbol{A}^{\mathrm{T}}\delta\boldsymbol{r}-\boldsymbol{n}^{\mathrm{T}}\delta\boldsymbol{r}'\right)\mathrm{d}s+\delta\boldsymbol{r}_{P}^{\mathrm{T}}\left[-(m_{P}+\mu\xi)\boldsymbol{A}_{P}-\mu\dot{\xi}^{2}\frac{\partial\boldsymbol{r}(\xi)}{\partial s}+\boldsymbol{F}_{P}\right]$$
$$+\delta\boldsymbol{r}_{C}^{\mathrm{T}}[-m_{B}\boldsymbol{A}_{B}+\boldsymbol{F}_{B}]+\delta\varphi[-I_{B}\ddot{\varphi}+M_{B}]=0 \tag{5.14}$$

Moreover, to simplify the discretization of the tether, the nondimensional unstrained arc-length coordinate $\bar{s}$ is introduced:

$$\bar{s}=\frac{1}{l_{0}}(s-\xi) \tag{5.15}$$

where l_{0} is the unstrained length of the deployed tether and satisfies $l_{0}=L-\xi$. Using this method, the solving domain is transformed from $[\xi,L]$ to $[0,1]$. To facilitate the discrimination, the position vector $\boldsymbol{r}$ and maneuvering acceleration $\boldsymbol{A}$ which are described by the nondimensional coordinate $\bar{s}$ are written as $\bar{\boldsymbol{r}}$ and $\bar{\boldsymbol{A}}$. Similarly, the coordinates x and z are also written as $\bar{x}$ and $\bar{z}$. By inserting Eq. (5.14), Eq. (5.15) can be written as:

$$\int_{0}^{1}\left(-\mu l_{0}\overline{\boldsymbol{A}}^{\mathrm{T}}\delta\bar{\boldsymbol{r}}-\boldsymbol{n}^{\mathrm{T}}\delta\bar{\boldsymbol{r}}'\right)\mathrm{d}s+\delta\boldsymbol{r}_{P}^{\mathrm{T}}\left[-(m_{\mathrm{P}}+\mu\xi)\boldsymbol{A}_{P}-\frac{\mu\dot{\xi}^{2}}{l_{0}}\boldsymbol{r}'(0)+\boldsymbol{F}_{P}\right]$$
$$+\delta\boldsymbol{r}_{C}^{\mathrm{T}}[-m_{B}\boldsymbol{A}_{B}+\boldsymbol{F}_{B}]+[-I_{B}\ddot{\varphi}+M_{B}]\delta\varphi=0 \tag{5.16}$$

where $\overline{\boldsymbol{A}} = \left[\overline{A}_x \;\; \overline{A}_z\right]^{\mathrm{T}}$, $\bar{A}_x$ and $\bar{A}_z$ are the components of the maneuvering acceleration $\boldsymbol{A}$ along the x_o axis and the z_o axis, which can be expressed as:

$$\begin{aligned}\overline{A}_x &= \ddot{\overline{x}} + 2(1-\bar{s})\frac{\dot{l}_0}{l_0}\dot{\overline{x}}' + (1-\bar{s})^2\frac{\dot{l}_0^2}{l_0^2}\overline{x}'' + (1-\bar{s})\frac{\ddot{l}_0}{l_0}\overline{x}' - 2(1-\bar{s})\frac{\dot{l}_0^2}{l_0^2}\overline{x}' \\ &\quad - 2\boldsymbol{\omega}\left[\dot{\overline{z}} + \frac{\dot{l}_0}{l_0}(1-\bar{s})\overline{z}'\right] \\ \overline{A}_z &= \ddot{\overline{z}} + 2(1-\bar{s})\frac{\dot{l}_0}{l_0}\dot{\overline{z}}' + (1-\bar{s})^2\frac{\dot{l}_0^2}{l_0^2}\overline{z}'' + (1-\bar{s})\frac{\ddot{l}_0}{l_0}\overline{z}' \\ &\quad - 2(1-\bar{s})\frac{\dot{l}_0^2}{l_0^2}\overline{z}' + 2\boldsymbol{\omega}\left[\dot{\overline{x}} + \frac{\dot{l}_0}{l_0}(1-\bar{s})\overline{x}'\right] - 3\boldsymbol{\omega}^2\overline{z}\end{aligned}$$

5.1.2 Mathematical Discretization

Although Eq. (5.16) can be used to describe the motion of the TSR system by a set of partial differential equations, it cannot be directly employed to design the coordinated controller and needs to be simplified.

The elastic stiffness of the material used in the braiding of the space tether is usually very high. For example, Young's module of the widely used Kevlar fiber is more than 100 Gpa. Besides, a structure braided with several fibers will further enhance the elastic stiffness and also have a good damping effect on the longitudinal vibration along the tether. On the other hand, compared with the tethered satellite systems, the tether length of the TSR system is only relatively short, only several kilometers long at most. Meanwhile, to avoid a big disturbance on the motion of the operation robot, the tension along the tether should be limited below a small value, even though the existence of the tension is inevitable due to the passive deployment mechanism. Thus two extra assumptions about the tether are made:

(1) Given the inner tension along the tether, the deployed tether can be regard to be approximately treated as a line in shape, which means the linear interpolating functions can be used to approximate it;

(2) The elastic stiffness is high enough so that the longitudinal deformation can be ignored. Therefore in the derivation, E is regarded as ∞ and ε zero.

According to the first assumption, the position vector of a point on the tether approximately satisfies the equation:

$$\boldsymbol{r}(\bar{s}, t) \approx \left[1-\bar{s} \;\; \bar{s}\right]\begin{bmatrix}\boldsymbol{r}_{\mathrm{P}}(t) \\ \boldsymbol{r}_{\mathrm{C}}(t)\end{bmatrix} \tag{5.17}$$

According to the definition of the orbital frame, the position vector $\boldsymbol{r}_{\mathrm{P}}$ can be calculated as:

$$\boldsymbol{r}_{\mathrm{P}}(t)=\begin{bmatrix}x_{\mathrm{P}}\\ z_{\mathrm{P}}\end{bmatrix}\equiv\begin{bmatrix}0\\ 0\end{bmatrix} \tag{5.18}$$

As shown in Fig. 5.1, the mass center of the operation robot can be calculated as:

$$\boldsymbol{r}_{\mathrm{B}}=\boldsymbol{r}_{\mathrm{C}}+\vec{CB}=\begin{bmatrix}x_{\mathrm{C}}+d\cos\varphi\\ z_{\mathrm{C}}-d\sin\varphi\end{bmatrix} \tag{5.19}$$

where $d=|\vec{CB}|$, φ is the angle between the x_B axis and the x_o axis. Inserting Eqs. (5.17)–(5.19) into Eq. (5.16) yields:

$$\begin{aligned}&\begin{bmatrix}\delta x_C\\ \delta z_C\end{bmatrix}^{\mathrm{T}}\left\{-\mu l_0\left\{\boldsymbol{M}\begin{bmatrix}\ddot{x}_C\\ \ddot{z}_C\end{bmatrix}+\left(2\frac{\dot{l}_0}{l_0}\boldsymbol{C}_1+\boldsymbol{C}_2\right)\begin{bmatrix}\dot{x}_C\\ \dot{z}_C\end{bmatrix}\right.\right.\\&\left.\left.+\left[\left(\frac{\ddot{l}_0}{l_0}-2\frac{\dot{l}_0^2}{l_0^2}\right)\boldsymbol{K}_1+\frac{\dot{l}_0}{l_0}\boldsymbol{K}_2+\boldsymbol{K}_3\right]\begin{bmatrix}x_C\\ z_C\end{bmatrix}\right\}\right.\\&\left.-\overline{N}\overline{\boldsymbol{\tau}}+\boldsymbol{R}_{\mathrm{F}}\begin{bmatrix}F_{Bx}\\ F_{Bz}\end{bmatrix}+\begin{bmatrix}C_x\\ C_z\end{bmatrix}\right\}+\left[-I_B\ddot{\varphi}+M_B+C_\varphi\right]\delta\varphi=0\end{aligned} \tag{5.20}$$

where $\boldsymbol{M}$ is the equivalent mass matrix, $\boldsymbol{C}_1$ and $\boldsymbol{C}_2$ are the equivalent damping matrixes, $\boldsymbol{K}_1$, $\boldsymbol{K}_2$, and $\boldsymbol{K}_3$ are the equivalent stiffness matrixes, they satisfy:

$$M=\begin{bmatrix}1/3+k & 0\\ 0 & 1/3+k\end{bmatrix},\quad C_1=\begin{bmatrix}-1/3 & 0\\ 0 & -1/3\end{bmatrix},$$

$$C_2=2\omega\begin{bmatrix}0 & -1/3-k\\ 1/3+k & 0\end{bmatrix}$$

$$K_1=\begin{bmatrix}-1/3 & 0\\ 0 & -1/3\end{bmatrix},\quad K_2=2\omega\begin{bmatrix}0 & 1/3\\ -1/3 & 0\end{bmatrix},\quad K_3=3\omega^2\begin{bmatrix}0 & 0\\ 0 & -1/3-k\end{bmatrix}$$

$\overline{N}$ and $\overline{\boldsymbol{\tau}}$ are the value and the unit direction vector of the equivalent tension along the tether:

$$\overline{N}=EA\left(\frac{l}{l_0}-1+\alpha\frac{\dot{l}l_0-l\dot{l}_0}{l_0^2}\right),\quad \overline{\boldsymbol{\tau}}=\left[\cos\theta\ \ -\sin\theta\right]^T$$

F_{Bx} and F_{Bz} are the components of the control force $\boldsymbol{F}_B$ along the x_B axis and the z_B axis. $\boldsymbol{R}_{\mathrm{F}}$ is the corresponding transformation matrix, which can be expressed as:

$$\boldsymbol{R}_{\mathrm{F}} = \begin{bmatrix} \cos\alpha & \sin\alpha \\ -\sin\alpha & \cos\alpha \end{bmatrix}$$

C_x and C_z are the coupling terms along the x_o axis and the z_o axis. C_φ is the coupling term around the y_B axis. They can be calculated as:

$$C_x = m_R\left(d\dot{\varphi}^2\cos\varphi + d\ddot{\varphi}\sin\varphi - 2\omega d\dot{\varphi}\cos\varphi\right)$$

$$C_z = m_R\left(-d\dot{\varphi}^2\sin\varphi + d\ddot{\varphi}\cos\varphi + 2\omega d\dot{\varphi}\sin\varphi - 3\omega^2 d\sin\varphi\right)$$

$$C_\varphi = -d_x(p_x\sin\varphi + p_z\cos\varphi)$$

Here, k is the mass ratio of the terminal operation mechanism to the deployed tether which can be expressed as:

$$k = \frac{m_B}{\mu l}$$

p_x and p_z are the components of the coupling force along the x_o axis and the z_o axis, which can be expressed as:

$$\begin{bmatrix} p_x \\ p_z \end{bmatrix} = \begin{bmatrix} -m_B(\ddot{x} - 2\omega\dot{z}) \\ -m_B\left(\ddot{z} + 2\omega\dot{x} - 3\omega^2 z\right) \end{bmatrix} + \boldsymbol{R}_{\mathrm{F}}\begin{bmatrix} F_{Bx} \\ F_{Bz} \end{bmatrix}$$

According to Eq. (5.20), the motion of the tether attachment point satisfies the equation:

$$\begin{aligned} &-\mu l_0\left\{\boldsymbol{M}\begin{bmatrix}\ddot{x}_C \\ \ddot{z}_C\end{bmatrix} + \left(2\frac{\dot{l}_0}{l_0}\boldsymbol{C}_1 + \boldsymbol{C}_2\right)\begin{bmatrix}\dot{x}_C \\ \dot{z}_C\end{bmatrix}\right. \\ &\left. + \left[\left(\frac{\ddot{l}_0}{l_0} - 2\frac{\dot{l}_0^2}{l_0^2}\right)\boldsymbol{K}_1 + \frac{\dot{l}_0}{l_0}\boldsymbol{K}_2 + \boldsymbol{K}_3\right]\begin{bmatrix}x_C \\ z_C\end{bmatrix}\right\} \\ &-\overline{N}\overline{\boldsymbol{\tau}} + \boldsymbol{R}_{\mathrm{F}}\begin{bmatrix}F_{Bx} \\ F_{Bz}\end{bmatrix} + \begin{bmatrix}C_x \\ C_z\end{bmatrix} = \boldsymbol{0} \end{aligned} \tag{5.21}$$

Similarly, the attitude motion of the terminal mechanism can be described by the following equation:

$$-I_B\ddot{\varphi} + M_B + C_\varphi = 0 \tag{5.22}$$

To further separate the transverse and longitudinal motions of the tether, the position of the tether attachment point C in polar coordinates can be obtained:

$$\begin{bmatrix} x_C \\ z_C \end{bmatrix} = \begin{bmatrix} l\cos\theta \\ -l\sin\theta \end{bmatrix} \tag{5.23}$$

where $l = |\overrightarrow{PC}|$, θ is the angle between vector $\overrightarrow{PC}$ and the x_o axis. Inserting Eq. (5.23) into Eq. (5.21) yields:

$$\begin{aligned} -\mu l_0 \Bigg\{ & \begin{bmatrix} \ddot{l} \\ l\ddot{\theta} \end{bmatrix} + (\boldsymbol{M}\boldsymbol{R}_2)^{-1}\boldsymbol{M}\boldsymbol{R}_3 \begin{bmatrix} 2\dot{l}\dot{\theta} \\ l\dot{\theta}^2 \end{bmatrix} + (\boldsymbol{M}\boldsymbol{R}_2)^{-1}\left(2\frac{\dot{l}_0}{l_0}\boldsymbol{C}_1 + \boldsymbol{C}_2\right)\boldsymbol{R}_2 \begin{bmatrix} \dot{l} \\ l\dot{\theta} \end{bmatrix} \\ & + (\boldsymbol{M}\boldsymbol{R}_2)^{-1}\left[\left(\frac{\ddot{l}_0}{l_0} - 2\frac{\dot{l}_0^2}{l_0^2}\right)\boldsymbol{K}_1 + \frac{\dot{l}_0}{l_0}\boldsymbol{K}_2 + \boldsymbol{K}_3\right]\boldsymbol{R}_1 l \Bigg\} \\ & - (\boldsymbol{M}\boldsymbol{R}_2)^{-1}\left\{N\boldsymbol{\tau}_n + \boldsymbol{R}_{\mathrm{F}}\begin{bmatrix} F_{Bx} \\ F_{Bz} \end{bmatrix} + \begin{bmatrix} C_x \\ C_z \end{bmatrix}\right\} = \boldsymbol{0} \end{aligned} \tag{5.24}$$

where $\boldsymbol{R}_1$, $\boldsymbol{R}_2$, and $\boldsymbol{R}_3$ are the corresponding transformation matrices which can be expressed as:

$$\boldsymbol{R}_1 = \begin{bmatrix} \cos\theta \\ -\sin\theta \end{bmatrix}, \quad \boldsymbol{R}_2 = \begin{bmatrix} \cos\theta & -\sin\theta \\ -\sin\theta & -\cos\theta \end{bmatrix}, \quad \boldsymbol{R}_3 = \begin{bmatrix} -\sin\theta & -\cos\theta \\ -\cos\theta & \sin\theta \end{bmatrix}$$

Also, according to the first assumption, the strain in the tether can be calculated as:

$$\varepsilon = \frac{l}{l_0} - 1 \tag{5.25}$$

According to the second assumption, $\varepsilon \approx 0$, which leads to another equation $l \approx l_0$. Since $\ddot{l}_0$ is treated as one of the control inputs in this study, the tether deploying acceleration needs to satisfy:

$$\ddot{l} = \ddot{l}_0 \tag{5.26}$$

Then the equation about $\ddot{l}$ in Eq. (5.25) would be meaningless and the equation about $\ddot{\theta}$ can be written as the following form:

$$m^* l\ddot{\theta} + m_B d\cos(\varphi - \theta)\ddot{\varphi} = F_\theta^* \tag{5.27}$$

where m^* and F_θ^* are the equivalent mass and force along the positive direction of θ which can be calculated as:

$$m^* = m_B + \frac{1}{3}\mu l$$

$$\begin{aligned} F_\theta^* = {} & F_{Bx}\sin(\varphi - \theta) - F_{Bz}\cos(\varphi - \theta) + m_B C_{2\theta} \\ & - 2m_B\dot{l}\dot{\theta} + 2m_B\omega\dot{l} + 3m^* l\omega^2\sin\theta\cos\theta \end{aligned}$$

Here, $C_{2\theta}$ is the low-order coupling term along the positive direction of θ which can be calculated as:

$$C_{2\theta} = d\sin(\varphi-\theta)\dot{\varphi}^2 - 2\omega d\sin(\varphi-\theta)\dot{\varphi} + 3\omega^2 d\cos\theta\sin\varphi$$

Rewriting Eq. (5.22) with Eq. (5.23) and Eq. (5.26) yields:

$$m_B l d\cos(\varphi-\theta)\ddot{\theta} + \left(I_B + m_B d^2\right)\ddot{\varphi} = M_{\varphi}^{*} \tag{5.28}$$

where M_{φ}^{*} is the equivalent torque about the y_B axis, which satisfies:

$$M_{\varphi}^{*} = F_{\mathrm{M}} d_{\mathrm{M}} + C_{2\varphi}$$

Here, F_{M} and d_{M} are the attitude control force for the operation robot and the length of the corresponding force arm, $C_{2\varphi}$ is the low-order coupling term about the y_B axis which can be calculated as

$$\begin{aligned} C_{2\varphi} = &- F_{Bz} d + m_B d\sin(\varphi-\theta)\ddot{l}_0 - 2m_B d\cos(\varphi-\theta)\dot{l}\dot{\theta} \\ &- m_B d\sin(\varphi-\theta)l\dot{\theta}^2 + 2\omega m_B d\cos(\varphi-\theta)\dot{l} \\ &+ 2\omega m_B d\sin(\varphi-\theta)l\dot{\theta} + 3\omega^2 m_B\left(d^2\sin\varphi\cos\varphi + ld\sin\theta\cos\varphi\right) \end{aligned}$$

The second order term $\ddot{\theta}$ and $\ddot{\varphi}$ can be gained by solving Eqs. (5.27) and (5.28) simultaneously, that is,

$$\begin{bmatrix} \ddot{\theta} \\ \ddot{\varphi} \end{bmatrix} = \begin{bmatrix} f_{\theta}\left(l, \dot{l}, \theta, \dot{\theta}, \varphi, \dot{\varphi}, \ddot{l}_0, F_{Bx}, F_{Bz}, F_{\mathrm{M}}\right) \\ f_{\varphi}\left(l, \dot{l}, \theta, \dot{\theta}, \varphi, \dot{\varphi}, \ddot{l}_0, F_{Bx}, F_{Bz}, F_{\mathrm{M}}\right) \end{bmatrix} \tag{5.29}$$

where f_{θ} and f_{φ} are the expressions of solutions. Thus the state equation of the tethered space robot system can be written as:

$$\dot{\boldsymbol{x}} = \boldsymbol{F}(\boldsymbol{x}, \boldsymbol{u}) \tag{5.30}$$

where $\boldsymbol{x}$ is the state vector, which can be expressed as:

$$\boldsymbol{x} = \left[l, \dot{l}, \theta, \dot{\theta}, \varphi, \dot{\varphi}\right]^{\mathrm{T}}$$

$\boldsymbol{u}$ is the control vector, which can be expressed as:

$$\boldsymbol{u} = \left[\ddot{l}_0, F_{Bx}, F_{Bz}, F_{\mathrm{M}}\right]^{\mathrm{T}}$$

$\boldsymbol{F}$ is the state function vector, which can be expressed as:

$$\boldsymbol{F} = \left[\dot{\theta}, f_{\theta}, \dot{\varphi}, f_{\varphi}, \dot{l}, \ddot{l}_0\right]^{\mathrm{T}}$$

In this way, a novel pose coupling dynamical model of the TSR system is obtained. Compared with the dynamical models used in the literature, it

focuses on the coupling between the position and attitude of the operation robot and the effect of the flexible tether on the position and attitude of the operation robot by considering the distributed mass of the tether and the distributed force acting the tether. This will improve the precision of the dynamical model and lay the foundation of the optimal coordinated control design in the following section.

5.2 OPTIMAL COORDINATED CONTROLLER

5.2.1 Minimum-Fuel Problem

The optimal trajectory design of the TSR for the approaching phase can be transformed to an optimal control problem: looking for the optimal control variable $\boldsymbol{u}(t) \in R^4$ which satisfies the constraints and minimizes fuel consumption. For the TSR system, the deploying acceleration of the tether is regulated by the deployment mechanism mounted on the space platform. Therefore when analyzing the fuel consumption, we only need to consider the other three control variables. Then, the performance index J can be written as:

$$J = \int_0^{t_f} \frac{1}{2}\left(F_{Bx}^2 + F_{Bz}^2 + F_{\mathrm{M}}^2\right)\mathrm{d}t \tag{5.31}$$

where t_f is the time for the whole approaching process.

Firstly, the constraints in state equation (5.30) should be satisfied. Secondly, the attitude of the terminal mechanism needs to meet the requirements as follows:

$$\varphi_{\min} \le \varphi \le \varphi_{\max} \tag{5.32}$$

where $\varphi_{\min}$ and $\varphi_{\max}$ are the lower and upper limits of the attitude angle, respectively. Thirdly, the control variables need to satisfy the following requirement:

$$\boldsymbol{u}_{\min} \le \boldsymbol{u}(t) \le \boldsymbol{u}_{\max} \tag{5.33}$$

where $\boldsymbol{u}_{\min}$ and $\boldsymbol{u}_{\max}$ are the lower limit and the upper limit of the control vector, respectively. Lastly, the whole system needs to meet the conditions of the initial launch and the final capture, which can be written as:

$$\boldsymbol{x}(0) = \boldsymbol{x}_0, \quad \boldsymbol{x}(t_\mathrm{f}) = \boldsymbol{x}_\mathrm{f} \tag{5.34}$$

where $\boldsymbol{x}_0$ and $\boldsymbol{x}_\mathrm{f}$ are the required initial state and the ideal final state, respectively.

5.2.2 Hp-Adaptive Pseudospectral Method

The hp-adaptive pseudospectral method is the combination of the classical Gauss pseudospectral method and the finite element method, which shows higher precision and faster velocity in solving nonsmooth optimization problems compared with the traditional pseudospectral methods. Considering the sudden change of the deploying acceleration and the thrust force, the hp-adaptive pseudospectral method is chosen to solve the minimum-fuel problem.

To solve the optimization problem formulated by Eqs. (5.31)–(5.34), the hp-adaptive pseudospectral method divides the whole period into several intervals and picks some Legendre-Gauss points as the collocation points in every interval. Then, the Lagrange polynomial is used to approximate the state variables and the control variables. The differential and integral of the interpolating functions are used to approximate the state differential and the performance index, which can transform the consecutive optimization problem into the discrete nonlinear programming problem. Lastly, the self-adapting collocation point adjustment strategy is introduced and the nonlinear programming problem can be solved by several kinds of traditional algorithm. In practice, the software GPOPS (Version 5.0) offered by Anil V. Rao is used [14–16].

5.2.3 Closed-Loop Controller

The optimal trajectory can be obtained by solving the minimum-fuel problem with the hp-adaptive pseudospectral method. To ensure the operation robot moves along the planned trajectory, the closed-loop controller is designed as shown in Fig. 5.2. It takes the open-loop state values and the input values corresponding to the optimal trajectory as the ideal state and input. However, if the ideal input is directly used to control the TSR system, errors will occur between the actual states and ideal states. Therefore the classical PD controller is used to reduce the errors, and the actual inputs are the sum of the ideal inputs and the output of the PD controller.

For the TSR system in the approaching phase, the length of deployed tether l is totally regulated by the deploying acceleration $\ddot{l}_0$. The tether angle θ is mainly controlled by the thrust F_x and F_z, and the attitude angle φ by the thrust F_M. Therefore the closed-loop control law can be written as:

$$\boldsymbol{u} = \boldsymbol{u}^* + \boldsymbol{R}_d \boldsymbol{K}_{PD}(\boldsymbol{x} - \boldsymbol{x}^*) \tag{5.35}$$

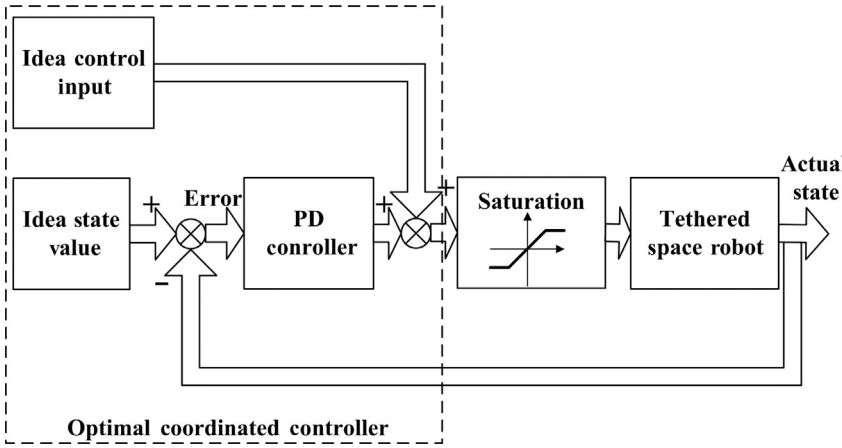

Fig. 5.2 Sketch map of closed-loop control system.

where $\boldsymbol{x}^*$ and $\boldsymbol{u}^*$ are the ideal state and input obtained in Section **5.2.2**, $\boldsymbol{R}_\mathrm{d}$ is the distribution matrix which can be calculated as:

$$\boldsymbol{R}_\mathrm{d} = \begin{bmatrix} 0 & 0 & 1 \\ \sin(\varphi-\theta) & 0 & 0 \\ \cos(\varphi-\theta) & 0 & 0 \\ 0 & 1 & 0 \end{bmatrix}$$

$\boldsymbol{K}_\mathrm{PD}$ is the parameter matrix of the PD controller which can be expressed as:

$$\boldsymbol{K}_\mathrm{PD} = \begin{bmatrix} k_{p\theta} & k_{d\theta} & 0 & 0 & 0 & 0 \\ 0 & 0 & k_{p\varphi} & k_{d\varphi} & 0 & 0 \\ 0 & 0 & 0 & 0 & k_{pl} & k_{dl} \end{bmatrix}$$

where $k_{p\theta}$, $k_{p\varphi}$, and k_{pl} are the proportional coefficients, $k_{d\theta}$, $k_{d\varphi}$, and k_{dl} are differential coefficients.

5.3 NUMERICAL SIMULATION

The TSR system is assumed to be in a circular orbit with a height of 500 km. The mass of the terminal operation mechanism is 2 kg with a moment of inertia 0.1 kg m^2. The linear density of the tether is 0.0045 kg/m. The distance between point C and point B is 0.3 m and the length of the force arm is 0.2 m. The deploying acceleration is limited in $[-0.2, 0.1]$ $\mathrm{m/s}^2$ and the maximum thruster force is 0.2 N.

To leave some margins for the on-line adjustment and prevent the closed-loop controller from getting saturated easily, the range of the deploying acceleration is strictly limited in $[-0.2, -0.02]$ m/s^2 when solving the minimum-fuel problem with the hp-adaptive pseudospectral method, and the maximum thruster force is 150 mN. Also, the range of the attitude angle is required to be in the range of $[-1°, 1°]$. The initial position and velocity of the terminal operation mechanism are $(1, 0, 0)^{\mathrm{T}}$ m and $(10, 0, 0)^{\mathrm{T}}$ m/s, respectively. The desired position and velocity of capturing are $(1000, 0, -1000)^{\mathrm{T}}$ m and $(0, 0, 0)^{\mathrm{T}}$ m/s, respectively.

To verify the performance of the closed-loop controller, 0.1 m initial deployed length deviation and 5° initial angle deviation are introduced in the simulation. Thus the initial position is set as $(1.0958, 0, -0.0959)$ m while the initial velocity remains unchanged.

To compare the proposed model with the traditional model based on the massless rod approximation, we use the hp-adaptive pseudospectral method to solve these two models under the same conditions. The solved optimal trajectories are both substituted into the model proposed in this study for simulation and the results are shown in Fig. 5.3. Since the massless rod model neglects the distributed mass of the tether and the distributed force acting on the tether, the final simulation result has a position error with 174 m which is far larger than the error of the proposed model (3.34 m) and cannot satisfy the requirements of the on-orbit servicing task.

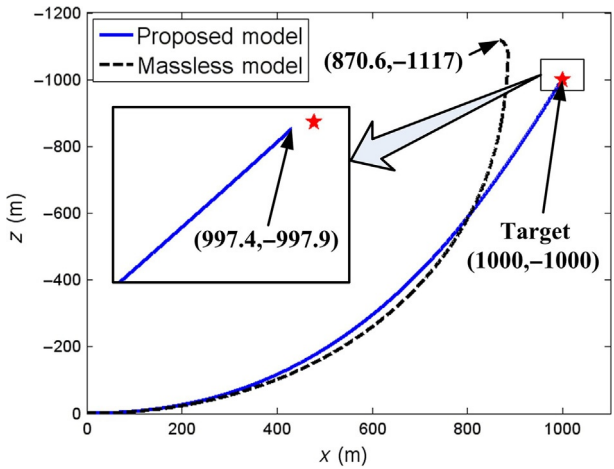

Fig. 5.3 Trail of terminal operation mechanism.

The proposed coordinated control method is compared with the traditional control method which uses the massless rod model and separately controls the position and attitude in Figs. 5.4 and 5.5. Fig. 5.4 illustrates the value of the control variables solved by the hp-adaptive pseudospectral method and Fig. 5.5 shows the comparison of the fuel consumption. From Fig. 5.5, we can know that two controllers both use the strategy of "decelerating-keeping-decelerating" for the tether control. The accelerations during the first period both are -0.2 m/s^2 because $|\theta - \varphi|$ is very small. But considering $|\theta - \varphi|$ increases with time, the duration of the first deceleration for the proposed coordinated controller is short for 2 s. During the second period of deceleration, since $|\theta - \varphi|$ is quite large, the proposed controller takes the strategy of decelerating slowly with more time (begin at 150 s and the acceleration gradually increases from -0.02 to -0.095 m/s^2), which can avoid the appearance of large attitude disturbance torque. However, the traditional controller still sets the acceleration as -0.2 m/s^2, which makes the attitude disturbance torque so large that it goes beyond the ability of the attitude control unit and leads to the divergence of the whole system. Moreover, from Fig. 5.5, we can know that even though the fuel

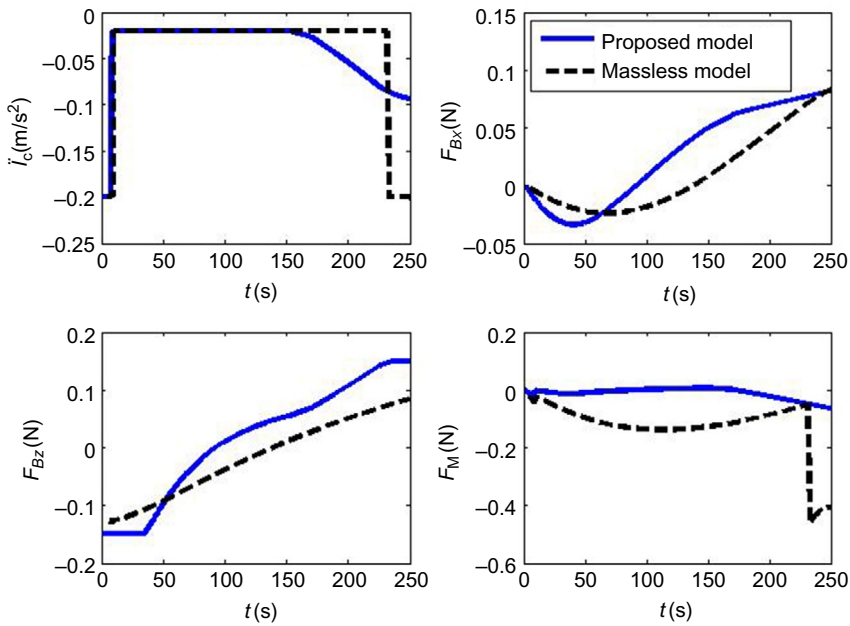

Fig. 5.4 Control law solved by pseudospectral method.

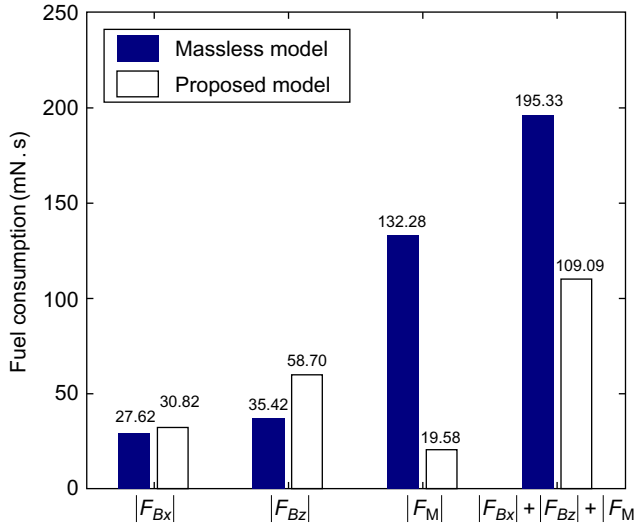

Fig. 5.5 Fuel consumption of thrusters.

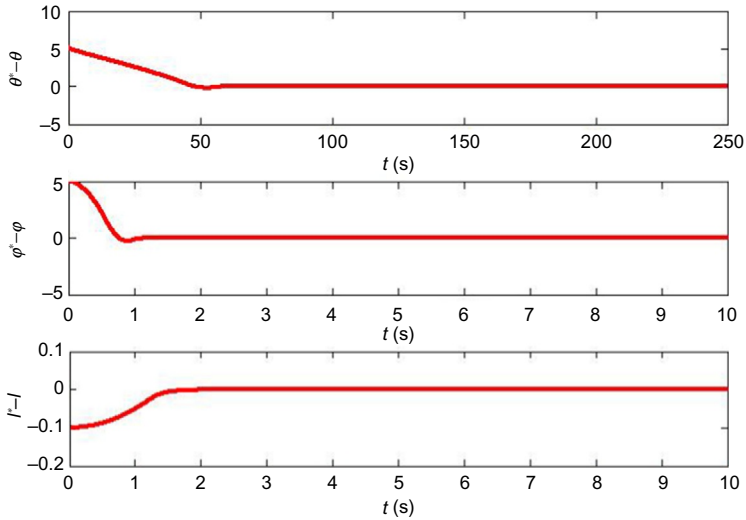

Fig. 5.6 Curve of state and error in closed-loop system.

consumption on F_{Bx} and F_{Bz} for the proposed coordinated controller are a little larger, the attitude controller consumes far less fuel than the traditional controller, and the whole fuel consumption is reduced by 40%.

The tracking errors in the closed-loop simulation are shown in Fig. 5.6, where θ^*, φ^*, and l^* are the desired value of θ, φ, and l, respectively. It can be

seen that under the control of the closed-loop controller, the initial state errors can be eliminated quickly and the system can track the desired states steadily, which verifies the validation of closed-loop controller.

From the above simulation results, it can be concluded that the optimal coordinated controller, which uses the deploying acceleration of the tether and the thrust on the operation robot as the system inputs, can not only minimize fuel consumption, but also avoid the appearance of large attitude disturbance torque.

REFERENCES

[1] M. Nohmi, Attitude control of a tethered space robot by link motion under microgravity, in: Proceedings of the 2004 IEEE International Conference on Control Applications, 2004, vol. 1, IEEE, 2004.

[2] Y. Nakamura, S. Fumiki, N. Shinichi, Guidance and control of tethered retriever with collaborative tension-thruster control for future on-orbit service missions, in: Proceedings of the 8th International Symposium on Artificial Intelligence, Robotics and Automation in Space (i-SAIRAS 2005), 2005.

[3] O. Mori, M. Saburo, Coordinated control of tethered satellite cluster systems, in: AIAA Guidance, Navigation, and Control Conference and Exhibit, Montreal, AIAA Paper, vol. 4392, 2001.

[4] Godard, K.D. Kumar, B. Tan, Fault-tolerant stabilization of a tethered satellite system using offset control, J. Spacecr. Rocket. 45 (5) (2008) 1070–1084.

[5] K.S. Anderson, P. Hagedorn, Control of orbital drift of geostationary tethered satellites, J. Guid. Control. Dyn. 17 (1) (1994) 10–14.

[6] A.K. Misra, Dynamics and control of tethered satellite systems, Acta Astronaut. 63 (11–12) (2008) 1169–1177.

[7] P. Williams, In-plane payload capture with an elastic tether, J. Guid. Control. Dyn. 29 (4) (2006) 810–821.

[8] T.S. No, J.E. Cochran Jr., Dynamics and control of a tethered flight vehicle, J. Guid. Control. Dyn. 18 (1) (1995) 66–72.

[9] A.K. Banerjee, Dynamics of tethered payloads with deployment rate control, J. Guid. Control. Dyn. 13 (4) (1990) 759–762.

[10] K.K. Mankala, S.K. Agrawal, Dynamic modeling and simulation of satellite tethered systems, J. Vib. Acoust. 127 (2) (2005) 144–156.

[11] M. Krupa, et al., Modeling, dynamics and control of tethered satellite systems, Nonlinear Dyn. 43 (1–2) (2006) 73–96.

[12] J.L. Tang, et al., Dynamics of variable-length tethers with application to tethered satellite deployment, Commun. Nonlinear Sci. Numer. Simul. 16 (8) (2011) 3411–3424.

[13] A. Kuhn, et al., A comparison of various mathematical formulations and numerical solution methods for the large amplitude oscillations of a string pendulum, Appl. Math. Comput. 67 (1) (1995) 227–264.

[14] D.A. Benson, et al., Direct trajectory optimization and costate estimation via an orthogonal collocation method, J. Guid. Control. Dyn. 29 (6) (2006) 1435–1440.

[15] D. Garg, W.W. Hager, A.V. Rao, Pseudospectral methods for solving infinite-horizon optimal control problems, Automatica 47 (4) (2011) 829–837.

[16] P. Williams, Optimal control of electrodynamic tether orbit transfers using timescale separation, J. Guid. Control. Dyn. 33 (1) (2010) 88–98.